**Proceedings of the ASME 2023**
**International Mechanical Engineering Congress and Exposition**
**IMECE2023**
**October 29-November 2, 2023, New Orleans, Louisiana**

**IMECE2023-111018**



# MODELING AND ANALYSIS OF TERRESTRIAL LOCOMOTION DYNAMICS OF HELICAL DRIVE-PROPELLED MULTI-TERRAIN VEHICLES

**Sumedh Beknalkar**
North Carolina State University
Raleigh, NC

**Aditya Varanwal**
North Carolina State University
Raleigh, NC

**Ryan Lynch**
North Carolina State University
Raleigh, NC

**Matthew Bryant**
North Carolina State University
Raleigh, NC

**Andre Mazzoleni**
North Carolina State University
Raleigh, NC

## ABSTRACT

*The diverse and heterogeneous terrains in the Arctic, consisting of snow, melting ice, permafrost, ice-covered lakes, sea ice and open ocean, pose serious challenges to locomotion and autonomous navigation capabilities of rovers deployed in the region for data collection and experimentation. The **M**ulti-terrain **A**mphibious **ARC**tic expl**O**rer or MAARCO rover is a proposed screw-propelled vehicle that uses helical drives (similar to Archimedes' screws) to move seamlessly across the diverse terrains in the Arctic. The motion of a pair of helical drives operating in soft or fluid terrain is dictated by the response of the surrounding substrate to the stresses exerted by the rotating helical drives. If the substrate under the rover does not fail when it is moving in a straight line, the linear displacement of the rover ($x$) and the number of rotations of the helical drives ($n$) are related through $x = P \cdot n$, where $P$ is the pitch length of the helical drives. However, when the substrate fails, the linear displacement of the rover is less than $P \cdot n$, i.e., $x < P \cdot n$. Thus, "$x = P \cdot n$" motion represents the optimal mode of operation for the rover when moving in a straight line. This paper represents the first ever attempt, to the best of author's knowledge, to derive the conditions necessary for the application of the holonomic constraint $x = P \cdot n$ to the dynamics of a helical drives-based rover.*

Keywords: planar locomotion dynamics, holonomic constraint, substrate failure check, multi-terrain, amphibious, helical drives, screw-propelled vehicle, Archimedes' screw, Arctic exploration

## 1. INTRODUCTION

Global warming has resulted in vast tracts of polar ice melting away leading to rising water levels and ever-changing weather patterns. The need to study the effects of global warming in the polar regions has led to the development of autonomous robots that can operate in areas that are inaccessible and dangerous to humans [1]-[3]. However, most robots developed so far have been deployed in areas of flat and mostly uniform terrain like the central plateau of the Antarctic continent. The diverse and heterogeneous terrains in the Arctic, consisting of snow, melting ice, permafrost, ice-covered lakes, sea ice and open ocean, pose serious challenges to locomotion and autonomous navigation capabilities that are not met by any current rover technology. A robot deployed in the Arctic must be highly adaptable to the diverse terrain conditions and must possess the ability to traverse both on land and under water.

This paper presents the study of terrestrial locomotion dynamics of a proposed multi-terrain and amphibious rover capable of moving seamlessly across the diverse terrains in the Arctic. The proposed rover – MAARCO (Multi-terrain Amphibious ARCtic explOrer) employs a propulsion system that consists of a pair of helical drives or Archimedes' screws. Helical drives are screw-like rotating central cylinders with helical blades. In snow, mud, and melting ice, the helical blades push the surface medium backward and produce propulsion. On water, the hollow central cylinders offer buoyancy that enables the vehicle to stay afloat while the rotating blades produce thrust. Conversely, the central cylinders can be flooded with water as ballast to make the vehicle neutrally buoyant for underwater operation, with thrust provided via the rotating blades. The variable buoyancy and combination of ground, ice, and water locomotion capabilities enable the MAARCO rover to traverse the heterogeneous landscape in the Arctic both on land and under water.

While helical drives have been demonstrated as propulsion mechanisms in manned vehicles for various

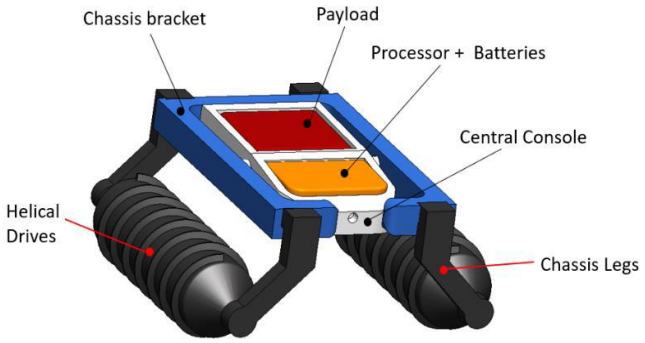


**FIGURE 1:** SCHEMATIC THE MAARCO AND ITS COMPONENTS

purposes, limited understanding of the dynamics of the helical drives, at the time, resulted in heavy and inefficient designs with low maximum speeds and high-power requirements. The advent of modern computational tools has led to a resurgence of attempts to analyze the terrestrial locomotion characteristics of helical drives in recent years [4-10]. Terrestrial locomotion of helical drives represents an involved dynamics problem that includes complex interaction between the surrounding substrate and helical drives. The motion of helical drives is dictated by how the surrounding substrate 'behaves' under the stresses exerted by the rotating helical drives. Whether the substrate fails or stays intact under the stresses exerted by the helical drive determines the locomotion of a helical drive propulsion system. Specifically, the velocity of the point of contact of the blade with the surface medium in a direction perpendicular to the face of the blade is either zero or non-zero depending on the whether substrate between the blades failing or not. When the rover is moving in a straight line (counter-rotating helical drives acted upon by the equal amounts of torque) without failing the substrate, the velocity constraint can be simplified to $x = P \cdot n$ or $x = P \cdot \theta/2\pi$, where $x$ is the linear displacement of the center of mass of the rover, and $P$, $n$, and $\theta$ are the pitch length, number of rotations, and angular displacement of the helical drives, respectively. Thus, the motion of the rover resembles that of a "bolt through a threaded hole" while moving in a straight line when the surrounding substrate does not fail. The holonomic constraint $x = P \cdot n$ if valid can then be applied to the locomotion dynamics model of a helical drives-based rover to eliminate a degree of freedom or dependent variable. However, when the substrate fails, the linear displacement of helical drive is less than $P \cdot n$, i.e., $x < P \cdot n$ This paper represents the first ever attempt, to the best of author's knowledge, to derive the conditions necessary for the application of the holonomic constraint to the dynamics of a helical drives-based rover or a screw-propelled vehicle.

The rest of the paper is organized as follows: In Section 2, first, we derive a simplified planar model of the locomotion of dynamics of the MAARCO rover. Second, we focus on rover dynamics involved in moving in a straight line, particularly, the holonomic constraint that is applied to the dynamic model when the substrate does not fail. Then, we derive the conditions necessary for substrate failure under the stresses exerted by the helical drives. In Section 3, we discuss the results of the simulation of the MAARCO rover moving along a straight line and check for the substrate failure criterion.

## 2. METHODS and MODELING

### 2.1 System Description

Fig. 1 shows a schematic of the proposed MAARCO rover. The rover consists of a pair of helical drives, a central console, and a chassis which consists of a chassis bracket and four chassis legs. The central console carries the payload that includes sensors, control and communications electronics, batteries, and/or solar panels, and sample collectors. The chassis legs can be raised or lowered relative to the central console to change the ground clearance and location of the rover center of mass. The helical drives may be partially or fully submerged into the surrounding medium depending on the surface and bulk characteristics of the medium and the overall weight and design of the rover. The torques acting on the helical drives control the angular accelerations of the helical drives. Using a differential steering system, the vehicle is able to track different paths such as moving along a straight line, turning left, and turning right. The relative angular displacement of the helical drives determines the direction of motion and orientation of the rover.

### 2.2 System Dynamics

In this work, a planar or two-dimensional model of the terrestrial locomotion dynamics of MAARCO has been considered; in that the rover is assumed to be moving in the $X$-$Y$ plane (Fig. 2). The two helical drives are in contact with the ground, and it is assumed that all the external forces exerted by the surrounding substrate act through a single point on the surface of the helical drive. In dynamically modeling the system, a multi-body system with 3 bodies – one central console and two helical drives, is considered. The model assumes that the chassis legs have small enough inertia so as to have a negligible impact on the overall dynamics of the rover. Multi-body dynamic

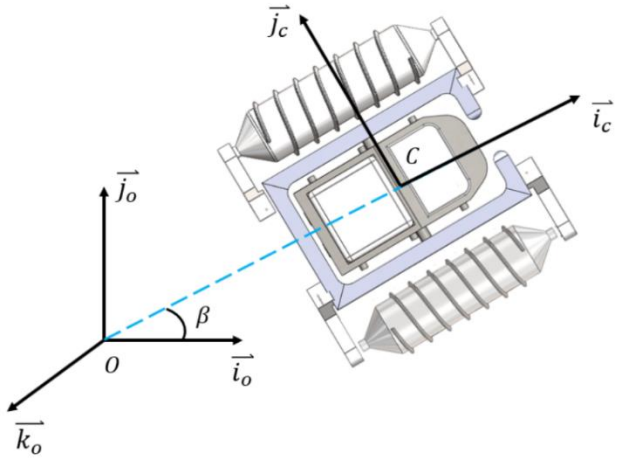


**FIGURE 2:** SCHEMATIC OF THE PLANAR MODEL OF MAARCO ALONG WITH the INERTIAL REFERENCE FRAME (IRF), $\bar{O}$, AND BODY FRAME, $\bar{C}$

systems, such as the MAARCO rover, have been modeled using various analytical techniques such as the Newton-Euler method and the Lagrange's Equations. In this work, the Newton-Euler approach has been used to derive the equations of motion of the system. The system has three degrees of freedom – $X$ and $Y$ coordinates of the rover center of mass and the orientation of the rover body axis (located at the center of mass) with respect to the inertial reference frame. The analytical governing equations of motion obtained using the Newton-Euler approach are integrated numerically to derive the time response of the system.

### 2.3 Definition of Frames

The first step in developing a dynamic model of a system is the definition of the frames used in the analysis. The frames used in this derivation are defined using their respective origins, unit vectors, and, for the body frames, the body that they are embedded in. As shown in Fig. 2, the frame $\bar{O}$ with $O$ at its origin is the arbitrarily located inertial reference frame (IRF). The unit vectors $\vec{\imath}_{\bar{o}}$ and $\vec{\jmath}_{\bar{o}}$ lie in the plane of the page with $\vec{k}_{\bar{o}}$ coming out of the page. The body frame $\bar{C}$ with unit vectors $\vec{\imath}_c, \vec{\jmath}_c, \vec{k}_{\bar{c}}$ has its origin at point $C$ which is the center of mass of the rover ($CM = C$, where $CM$ is the center of the mass of the rover). Frame $\bar{C}$ is derived through a rotation about $\vec{k}_{\bar{o}} = \vec{k}_c$ axis by an angle of $\beta = \beta(t)$. The center of masses of the left and right helical drives are located at points $HL$ and $HR$, respectively. The frames that rotate along with the helical drives are shown in Fig. 3. The frames located at points $HL$ and $HR$ are obtained through the clockwise and counterclockwise rotation about the $\vec{\imath}_c$ axis at angles of $\theta_L$ and $\theta_R$ respectively, where $\theta_L$ and $\theta_R$ are angular positions of the left and right helical drives. Points $L_{\theta_L}$ and $R_{\theta_R}$ are arbitrary points located on the surface of the left and right helical drives that rotate along with the rotating helical drives. Points $L$ and $R$ are derived using points $L_{\theta_L}$ and $R_{\theta_R}$ such that $\theta_L = 0$ and $\theta_R = 0$, respectively. Points $L$, and $R$ are located at a distance of $r$ from $HL$ and $HR$, respectively, where $r$ represents the effective radius of the helical drives. The forces acting on the helical drives are assumed to act through points $L$ and $R$. Another set of frames are required to define the forces acting normal and tangential to the helical drive blades. As shown in Fig. 4, these frames are derived through a fixed angle rotation of $-\varphi$ and $\varphi$ about the $\vec{k}_c$ for the left and right helical drives respectively. It is important to note that the helical blades depicted in all the figures are on the bottom/lower half of the helical drives and are in contact with the surrounding substrate.

### 2.4 Forces acting on Helical Drives

1. *Force acting normal to the ground* ($\overrightarrow{N_g}$)

This normal force is exerted by the ground on the rover and acts in a direction perpendicular to the surface. The ground is assumed to be flat and uniform and lies in the $X-Y$ plane. Hence, $\overrightarrow{N_g}$ acts along $\vec{k}_{\bar{o}}$ (or $\vec{k}_{\bar{o}}$), i.e.,

$$\overrightarrow{N_g} = N_g\vec{k}_{\bar{o}} = N_g\vec{k}_c \tag{1}$$

where, $N_g$ is the magnitude of the normal force.

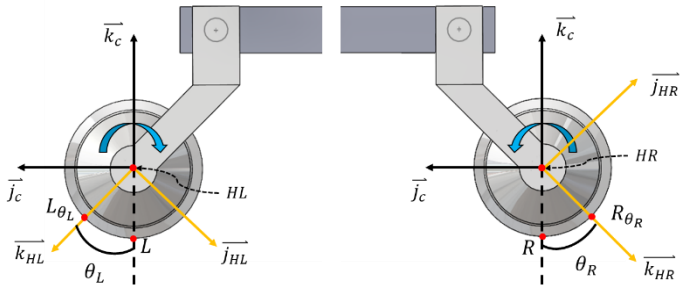


**FIGURE 3:** FRAMES $\overline{HL}$ AND $\overline{HR}$ ROTATE ALONG WITH THE LEFT AND RIGHT HELICAL DRIVES, RESPECTIVELY

2. *Friction force due to* $\overrightarrow{N_g}$ ($\overrightarrow{F_{L1}}$ or $\overrightarrow{F_{R1}}$)

This force acts on the central cylinder or ballast of the helical drive opposing the linear motion of the point L or R on the helical drive. The motion of L and R on the respective helical drive is a combination of the motions due to the rotating ballast and the forward moving rover. When the rover moves forward (along $\vec{\imath}_{\bar{c}}$), the left (or right) helical drive rotates about $\vec{\imath}_c$ (or $-\vec{\imath}_c$) and translates linearly along $\vec{\imath}_c$ (or $\vec{\imath}_c$). The friction force acts in a direction opposite to the angle $\phi_{L\,or\,R}$ relative to $\vec{\jmath}_c$ (or $-\vec{\jmath}_c$) where $\tan(\phi_{L\,or\,R})$ is equal to the ratio of the linear speed of the rover and the rotational speed of the ballast, as shown in Fig. 5 for left helical drive..

3. *Force acting normal to the helical blades* ($\overrightarrow{N_L}$ or $\overrightarrow{N_R}$)

This propulsive force acts normal to the helical blades on the left (along $\vec{\imath}_L$) and right (along $\vec{\imath}_R$) helical drives. It is a reaction force exerted by the surrounding substrate on the helical drive that results in forward motion. The magnitude of this force depends on the bulk properties of the surrounding substrate and the dimensions and motion of the drives.

4. *Friction force due to normal (or propulsive) force* $\overrightarrow{N_L}$ or $\overrightarrow{N_R}$ ($\overrightarrow{F_{L2}}$ or $\overrightarrow{F_{R2}}$)

Like the friction force due to $\overrightarrow{N_g}$, this force opposes the linear motion of the point L or R on the helical drive. It acts in the same direction as the friction force due to $\overrightarrow{N_g}$ (as shown in Fig. 5), except that it acts on the helical blades (instead of the ballast). However, in the simplified model discussed in this paper, both sets of friction forces are assumed to act through points L and R.

It is important to note that the friction forces are kinetic friction forces of the form: $F_k = \mu \cdot F_{normal}$, where $F_k$ is the magnitude of kinetic friction, $\mu$ is the coefficient of kinetic friction, and $F_{normal}$ is the normal force.

### 2.5 Deriving the Equations of Motion

Using the Newton-Euler approach, the equations of motion for the system are derived to solve for the degrees of freedom – the position of center of mass and the orientation of the rover in the $X-Y$ plane. First, we start by defining the position vector of the center of mass of the rover or point $C$ with respect to point $O$ in the IRF.

$$\vec{r}_{C/O} = x_c\vec{\imath}_o + y_c\vec{\jmath}_o \tag{2}$$

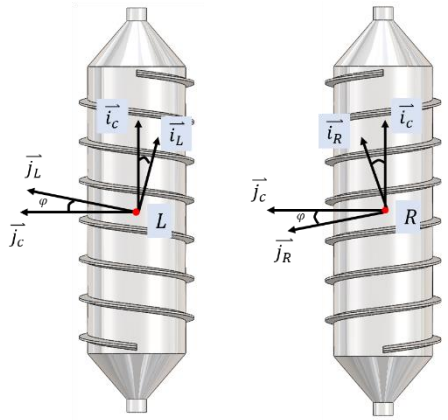


**FIGURE 4:** FRAMES $\bar{L}$ AND $\bar{R}$ ARE USED TO DEFINE FORCES ACTING NORMAL AND TANGENTIAL TO THE BLADES (THE BLADES SHOWN HERE ARE LOCATED ON BOTTOM HALF OF THE HELICAL DRIVES OR THE PART OF THE HELICAL DRIVES THAT IS IN CONTACT WITH THE SUSBTRATE)

Similarly, the velocity and acceleration vectors of point $C$ in the IRF are ${}^{\bar{O}}\vec{v}_{C/O} = \dot{x}_c\vec{\imath}_o + \dot{y}_c\vec{\jmath}_o$ and ${}^{\bar{O}}\vec{a}_{C/O} = \ddot{x}_c\vec{\imath}_o + \ddot{y}_c\vec{\jmath}_o$, respectively. The direction cosine matrix between the IRF ($\bar{O}$) and body frame $\bar{C}$ is:

$$\bar{C}[c]\bar{O} = \begin{bmatrix} \cos\beta & \sin\beta & 0 \\ -\sin\beta & \cos\beta & 0 \\ 0 & 0 & 1 \end{bmatrix} \quad (3)$$

Where, $\beta$ is the angle of rotation between the IRF ($\bar{O}$) and body frame $\bar{C}$ about the $\vec{k}_o$axis. Thus, the acceleration of point $C$ ($\vec{a}_{C/O}$), in the body frame will be:

$$\left\{{}^{\bar{O}}\vec{a}_{C/O}\right\}_{\bar{C}} = (\ddot{x}_c\cos\beta + \ddot{y}_c\sin\beta)\vec{\imath}_c + (-\ddot{x}_c\sin\beta + \ddot{y}_c\cos\beta)\vec{\jmath}_c \quad (4)$$

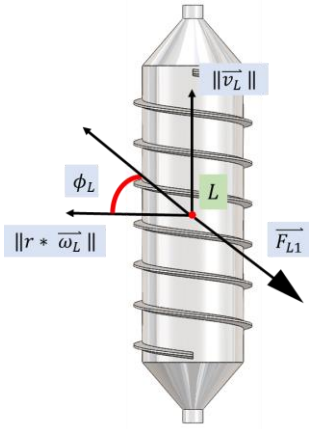


**FIGURE 5:** FRICTION FORCE DUE $\overrightarrow{N_g}$ ACTING ON THE LEFT HELICAL DRIVE

Now, let's consider the external forces acting on the rover system. The expression for $\overrightarrow{N_g}$ is shown in Equation (1). The friction force due to $\overrightarrow{N_g}$ acting on the ballast of left and right helical drives is derived as:

$$\overrightarrow{F_{L1}} = F_{L1}(-sin\phi_L\,\vec{\imath}_c - cos\phi_L\,\vec{\jmath}_c) \quad (5)$$
$$\overrightarrow{F_{R1}} = F_{R1}(-sin\phi_R\,\vec{\imath}_c + cos\phi_R\,\vec{\jmath}_c) \quad (6)$$

The force acting normal to the blades on the left and right helical drive is derived as:

$$\overrightarrow{N_L} = N_L\vec{\imath}_L = N_L(cos\varphi\,\vec{\imath}_c - sin\varphi\,\vec{\jmath}_c) \quad (7)$$
$$\overrightarrow{N_R} = N_R\vec{\imath}_R = N_R(cos\varphi\,\vec{\imath}_c + sin\varphi\,\vec{\jmath}_c) \quad (8)$$

Similarly, the friction force acting on the blades on the left and right helical drives is derived as:

$$\overrightarrow{F_{L2}} = F_{L2}\vec{\jmath}_L = F_{L2}(-sin\varphi\,\vec{\imath}_c - cos\varphi\,\vec{\jmath}_c) \quad (9)$$
$$\overrightarrow{F_{R2}} = F_{R2}\vec{\jmath}_L = F_{R2}(-sin\varphi\,\vec{\imath}_c + cos\varphi\,\vec{\jmath}_c) \quad (10)$$

Additionally, the weight of rover $\overrightarrow{F_g}$ is:

$$\overrightarrow{F_g} = -m_{rover}g\vec{k}_{\bar{o}} \quad (11)$$

where, $g$ is acceleration due to gravity and $m_{rover}$ is the total mass of the rover, which consists of the mass of the central console ($m_{cc}$) and the masses of two helical drives ($2 * m_{HD}$), where $m_{HD}$ is the mass of each helical drive. Therefore,

$$m_{rover}=(m_{cc} + 2 * m_{HD}) \quad (12)$$

Combining all the external forces, we get:

$$\left\{\overrightarrow{F_{ext}}\right\}_{\bar{C}} = \overrightarrow{N_L} + \overrightarrow{N_R} + \overrightarrow{F_{L1}} + \overrightarrow{F_{R1}} + \overrightarrow{F_{L2}} + \overrightarrow{F_{R2}} + \overrightarrow{N_g} + \overrightarrow{F_g} \quad (13)$$

$$\left\{\overrightarrow{F_{ext}}\right\}_{\bar{C}} = [N_L cos\varphi + N_R cos\varphi - F_{L1}sin\phi_L - F_{R1}sin\phi_R - F_{L2}sin\varphi - F_{R2}sin\varphi]\vec{\imath}_{\bar{c}} + [-N_L\,sin\varphi + N_R\,sin\varphi - F_{L1}\,cos\phi_L + F_{R1}cos\phi_R - F_{L2}cos\varphi + F_{R2}cos\varphi]\vec{\jmath}_c + [N_g + F_g]\vec{k}_{\bar{o}} \quad (14)$$

Using Newton's second law of motion equation for the rover system $\left\{\overrightarrow{F_{ext}}\right\}_{\bar{C}} = m_{rover} \cdot \left\{{}^{\bar{O}}\vec{a}_{C/O}\right\}_{\bar{C}}$, and comparing coefficients of $\vec{\imath}_c$, $\vec{\jmath}_c$, and $\vec{k}_c$we get:

For $\vec{\imath}_c$,

$$N_L cos\varphi + N_R cos\varphi - F_{L1}sin\phi_L - F_{R1}sin\phi_R - F_{L2}sin\varphi - F_{R2}sin\varphi = (m_{cc} + 2 * m_{HD}) * (\ddot{x}_c\cos\beta + \ddot{y}_c\sin\beta) \quad (15)$$

For $\vec{\jmath}_c$,

$$-N_L sin\varphi + N_R sin\varphi - F_{L1}cos\phi_L + F_{R1}cos\phi_R - F_{L2}cos\varphi + F_{R2}cos\varphi = (m_{cc} + 2 * m_{HD}) * (-\ddot{x}_c\sin\beta + \ddot{y}_c\cos\beta) \quad (16)$$

For $\vec{k}_c$,

$$N_g = -F_g = m_{rover}g = (m_{cc} + 2 * m_{HD})g \quad (17)$$

Equation 17 shows that the magnitude of the normal force ($N_g$) is equal to the weight of the rover. The normal force supports the

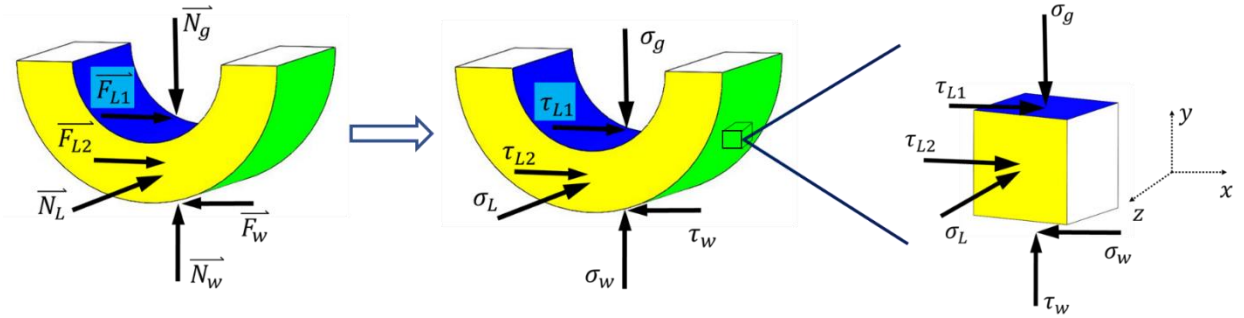


**FIGURE 6:** (FROM LEFT TO RIGHT) 1. FORCES ACTING ON ANNULAR SUBSTRATE ELEMENT LOCATED BETWEEN TWO BLADES, (2) STRESSES ACTING ON ANNULAR SUBSTRATE ELEMENT, (3) STRESSES ACTING ON CUBE-SHAPED SUBSTRATE ELEMENT

weight of the rover equally through points $L$ and $R$. So, the friction forces due to $\overrightarrow{N_g}$ acting on the ballast of left and right helical drives can be expressed as:

$$\overrightarrow{F_{L1}} = 0.5\, m_{rover}\, g\, \mu_{k1}(-sin\phi_L\, \vec{\imath}_c - cos\phi_L\, \vec{\jmath}_c) \quad (18)$$

$$\overrightarrow{F_{R1}} = 0.5\, m_{rover}\, g\, \mu_{k1}(-sin\phi_L\, \vec{\imath}_c + cos\phi_L\, \vec{\jmath}_c) \quad (19)$$

where, $\mu_{k1}$ is the kinetic friction between the substrate and helical drives.

Similarly, the friction forces acting on the helical blades on the left and right helical drives can be expressed as:

$$\overrightarrow{F_{L2}} = \mu_{k1} N_L(-sin\varphi\, \vec{\imath}_c - cos\varphi\, \vec{\jmath}_c) \quad (20)$$

$$\overrightarrow{F_{R2}} = \mu_{k1} N_R(-sin\varphi\, \vec{\imath}_c + cos\varphi\, \vec{\jmath}_c) \quad (21)$$

Now, let's calculate the external torques acting on the system, or specifically the torques exerted by the external forces listed in Equations 1, and 5 through 10. To calculate the external torques, the position vectors of $L$ and $R$ with respect to point $C$ are derived:

$$\vec{r}_{L/C} = w\vec{\jmath}_c - r\,\vec{k}_{\bar{c}} \quad (22)$$

$$\vec{r}_{R/C} = -w\vec{\jmath}_c - r\vec{k}_{\bar{c}} \quad (23)$$

where, $w$ is the distance between the center of masses of the rover and the individual helical drives and $r$ is the effective radius of the helical drives. So, the external torques acting on the rover system about its center of mass is:

$$\left(\vec{\tau}_{C,sys}\right)_{ext} = \vec{r}_{L/C} \times \left(\overrightarrow{N_L} + \overrightarrow{F_{L1}} + \overrightarrow{F_{L2}} + 0.5 * \overrightarrow{N_g}\right) + \vec{r}_{R/C} \times \left(\overrightarrow{N_R} + \overrightarrow{F_{R1}} + \overrightarrow{F_{R2}} + 0.5 * \overrightarrow{N_g}\right) \quad (24)$$

$$\begin{aligned}\left(\vec{\tau}_{C,sys}\right)_{ext} = {} & [(0.5wN_g) - (0.5wN_g) - (rF_{L1}cos(\phi_L)) \\ & + (rF_{R1}cos(\phi_R)) - (rF_{L2}cos(\psi)) \\ & + (rF_{R2}cos(\psi)) - (rN_L sin(\psi)) \\ & + (rN_R sin(\psi))]\vec{\imath}_{\bar{c}} + r[-(N_L\cos(\psi)) \\ & - (N_R\cos(\psi)) + \left(F_{L1}sin(\phi_L)\right) \\ & + \left(F_{R1}sin(\phi_R)\right) + (F_{L2}sin(\psi)) \\ & + (F_{R2}sin(\psi))]\vec{\jmath}_{\bar{c}} + w[-(N_L\cos(\psi)) \\ & + (N_R\cos(\psi)) + \left(F_{L1}sin(\phi_L)\right) \\ & - \left(F_{R1}sin(\phi_R)\right) + (F_{L2}sin(\psi)) \\ & - (F_{R2}sin(\psi)]\vec{k}_{\bar{c}}\end{aligned} \quad (25)$$

The external torque acting on a system about an arbitrary point $A$ ($\left(\vec{\tau}_{A,sys}\right)_{ext}$) is related to the change in angular momentum of the system about point $A$ as follows:

$$\left(\vec{\tau}_{A,sys}\right)_{ext} = {}^{\overline{O}}\frac{d}{dt}\left({}^{\overline{O}}_{O}h_{A,sys}\right) + {}^{\overline{O}}\vec{v}_{A/O} \times m_{sys}\, {}^{\overline{O}}\vec{v}_{CM/O} \quad (26)$$

where, $CM$ is the center of mass of the system. For the rover system under consideration $A = C$ and $CM = C$. So, the second term ${}^{\overline{O}}\vec{v}_{A/O} \times m_{sys}\, {}^{\overline{O}}\vec{v}_{CM/O} = {}^{\overline{O}}\vec{v}_{C/O} \times m_{sys}\, {}^{\overline{O}}\vec{v}_{C/O}$ is equal to $\vec{0}$. Now, using the appropriate notations, we get:

$$\left(\vec{\tau}_{C,sys}\right)_{ext} = {}^{\overline{O}}\frac{d}{dt}\left({}^{\overline{O}}_{O}h_{C,sys}\right) \quad (27)$$

Here, ${}^{\overline{O}}_{O}h_{C,sys}$ is the angular momentum of the system about point $C$ with respect to the IRF. Given that the location of the central console and helical drives does not change with respect to the center of mass and that the rover center of mass and point $C$ are one and the same, the angular momentum of the system can be simplified to:

$${}^{\overline{O}}_{O}h_{C,sys} = \tilde{I}_{C,sys} \cdot \bar{O}\vec{\omega}\bar{C} \quad (28)$$

where, $\tilde{I}_{C,sys}$ is the moment of inertia of the system about point $C$ and $\bar{O}\vec{\omega}\bar{C}$ is the angular velocity between the IRF and body frame $\overline{C}$. Given that frame $\bar{C}$ is derived through a rotation about $\vec{k}_{\bar{o}} = \vec{k}_c$ axis at an angle of $\beta$, we have:

$$\bar{O}\vec{\omega}\bar{C} = \dot{\beta}\vec{k}_{\bar{o}} = \dot{\beta}\vec{k}_{\bar{c}} \quad (29)$$

And,

$$\bar{O}\vec{\alpha}\bar{C} = \ddot{\beta}\vec{k}_{\bar{o}} = \ddot{\beta}\vec{k}_{\bar{c}} \quad (30)$$

So,

$$\left(\vec{\tau}_{C,sys}\right)_{ext} = {}^{\overline{O}}\frac{d}{dt}\left({}^{\overline{O}}_{O}h_{C,sys}\right) = {}^{\overline{O}}\frac{d}{dt}\left(\tilde{I}_{C,sys} \cdot \bar{O}\vec{\omega}\bar{C}\right) = \tilde{I}_{C,sys,z} \cdot \ddot{\beta}\,\vec{k}_{\bar{c}} \quad (31)$$

where, $\tilde{I}_{C,sys,z}$ is the moment of inertia of the system about $\vec{k}_{\bar{c}}$. Now, comparing the coefficients of $\vec{\imath}_c$, $\vec{\jmath}_c$, and $\vec{k}_c$ in Equation 25 and 31, we get:

For $\vec{\imath}_c$,

$$\begin{aligned} r[-F_{L1}cos(\phi_L) + F_{R1}cos(\phi_R) - F_{L2}cos(\psi) + F_{R2}cos(\psi) \\ - N_L sin(\psi) + N_R sin(\psi)] = 0 \end{aligned}$$

(32)

For $\vec{j}_c$,

$$r[-(N_L\cos(\psi)) - (N_R\cos(\psi)) + (F_{L1}sin(\phi_L)) + (F_{R1}sin(\phi_R)) + (F_{L2}sin(\psi)) + (F_{R2}sin(\psi))] = 0 \quad (33)$$

For $\vec{k}_c$,

$$w(-N_L cos\varphi + N_R cos\varphi + F_{L1}sin\phi_L - F_{R1}sin\phi_R + F_{L2}sin\varphi - F_{R2}sin\varphi) = \tilde{I}_{C,sys,k}\cdot\ddot{\beta} \quad (34)$$

Now, let's consider the motion of individual helical drives and the torques acting on each helical drive. As mentioned previously, the external forces act through points $L$ and $R$. So, first, the position vectors of $L$ and $R$ with respect to point $HL$ and $HR$ are derived as follows:

$$\vec{r}_{L/HL} = -r\,\vec{k}_{\bar{c}} \quad (35)$$

$$\vec{r}_{R/HR} = -r\,\vec{k}_{\bar{c}} \quad (36)$$

The external torques acting on the left helical drive about point $HL$ are:

$$\left(\vec{\tau}_{HL,HD}\right)_{ext} = \vec{r}_{L/HL}\times\left(\overrightarrow{N_L} + \overrightarrow{F_{L1}} + \overrightarrow{F_{L2}}\right) + \vec{\tau}_{motor,HL} + \vec{\tau}_{Joint\ forces,HL} \quad (37)$$

Similarly, external torques acting on the right helical drive about point $HR$ are:

$$\left(\vec{\tau}_{HR,HD}\right)_{ext} = \vec{r}_{R/HR}\times\left(\overrightarrow{N_R} + \overrightarrow{F_{R1}} + \overrightarrow{F_{R2}}\right) + \vec{\tau}_{motor,HR} + \vec{\tau}_{Joint\ forces,HR} \quad (38)$$

Here, $\vec{\tau}_{motor,HL}$ and $\vec{\tau}_{motor,HR}$ are user inputs to the system and represent driving torques exerted by the motors on the helical drives that result in helical drive rotation and consequently forward motion of the rover. $\overrightarrow{\vec{\tau}_{Joint\ forces,HL}}$ & $\vec{\tau}_{Joint\ forces,HR}$ are the torques due to the forces acting on the joints, exerted by the chassis legs on the helical drives,.

While applying Equation 26 for the left and right helical drives, we have $A = HL$, $CM = HL$, and $A = HR$, $CM = HR$, respectively. So, for the left helical drive, Equation 26 simplifies to:

$$\left(\vec{\tau}_{HL,HD}\right)_{ext} = \overline{O}\frac{d}{dt}\left(\overline{O}h_{HL,HD}\right) \quad (39)$$

Similarly, for the right helical drive:

$$\left(\vec{\tau}_{HR,HD}\right)_{ext} = \overline{O}\frac{d}{dt}\left(\overline{O}h_{HR,HD}\right) \quad (40)$$

Here, $\overline{O}h_{HL,HD}$ and $\overline{O}h_{HR,HD}$ are the angular momentums of the left and right helical drives about points $HL$ and $HR$ respectively with respect to the IRF. Given that the helical drives are rigid bodies and that their respective center of masses coincide with $HL$ and $HR$, the angular momentum of the left helical drive about $HL$ is:

$$\overline{O}h_{HL,HD} = \tilde{I}_{HL,HD}\cdot\bar{O}\vec{\omega}\overrightarrow{HL} \quad (41)$$

and the angular momentum of the right helical drive about $HR$ is:

$$\overline{O}h_{HR,HD} = \tilde{I}_{HR,HD}\cdot\bar{O}\vec{\omega}\overrightarrow{HR} \quad (42)$$

where, $\tilde{I}_{HL,HD}$ and $\tilde{I}_{HR,HD}$ are the moments of inertia tensor of the left and right helical drives about their centers of mass respectively whereas $\bar{O}\vec{\omega}\overrightarrow{HL}$ and $\bar{O}\vec{\omega}\overrightarrow{HR}$ are the angular velocity between the IRF and body frames located at points $HL$ and $HR$, respectively. The angular velocity terms can be derived using the following expressions:

$$\bar{O}\vec{\omega}\overrightarrow{HL} = \bar{O}\vec{\omega}\bar{C} + \bar{C}\vec{\omega}\overrightarrow{HL} = \dot{\beta}\vec{k}_{\bar{c}} + \dot{\theta}_L\vec{\imath}_{\bar{c}} \quad (43)$$

$$\bar{O}\vec{\omega}\overrightarrow{HR} = \bar{O}\vec{\omega}\bar{C} + \bar{C}\vec{\omega}\overrightarrow{HR} = \dot{\beta}\vec{k}_{\bar{c}} - \dot{\theta}_R\vec{\imath}_{\bar{c}} \quad (44)$$

So, the torques due to rate of change of angular momentums for both left and right helical drives are:

$$\left(\vec{\tau}_{HL,HD}\right)_{ext} = \overline{O}\frac{d}{dt}\left(\overline{O}h_{HL,HD}\right) = \overline{O}\frac{d}{dt}\left(\tilde{I}_{HL,HD}\cdot\bar{O}\vec{\omega}\overrightarrow{HL}\right) = \tilde{I}_{HL,HD}\cdot(\ddot{\beta}\vec{k}_{\bar{c}} + \ddot{\theta}_L\vec{\imath}_{\bar{c}}) + \left(I_{HL,HD,x} - I_{HL,HD,z}\right)\dot{\beta}\dot{\theta}_L\vec{J}_{\bar{c}} \quad (45)$$

$$\left(\vec{\tau}_{HR,HD}\right)_{ext} = \overline{O}\frac{d}{dt}\left(\overline{O}h_{HR,HD}\right) = \overline{O}\frac{d}{dt}\left(\tilde{I}_{HR,HD}\cdot\bar{O}\vec{\omega}\overrightarrow{HR}\right) = \tilde{I}_{HR,HD}\cdot(\ddot{\beta}\vec{k}_{\bar{c}} + \ddot{\theta}_L\vec{\imath}_{\bar{c}})\left(I_{HR,HD,x} - I_{HR,HD,z}\right)\dot{\beta}\dot{\theta}_L\vec{J}_{\bar{c}} \quad (46)$$

Now, comparing the coefficients of $\vec{\imath}_{\bar{c}}$, for Equations 39 and 45 (equations for left helical drives) we get:

$$r*(-N_L sin\varphi - F_{L1}cos\phi_L - F_{L2}cos\varphi) + \vec{\tau}_{motor,HL,x} = I_{HL,HD,x}\cdot\ddot{\theta}_L \quad (47)$$

and for Equations 40 and 46 (equations for right helical drives) we get:

$$r*(N_R sin\varphi + F_{R1}cos\phi_R + F_{R2}cos\varphi) + \vec{\tau}_{motor,HR,x} = -I_{HL,HD,x}\cdot\ddot{\theta}_R \quad (48)$$

It is important to note that the $torque\ due\ to\ joint\ forces$ act in such as a way to impose pitching and yawing motions on the helical drives, and not rolling. They act through the axis of rotation of the helical drives, i.e., $\vec{\imath}_{\bar{c}}$, and hence do not appear in Equations 47 and 48.

The planar locomotion model of the MAARCO rover discussed above has a total of fourteen dependent variables – $x_c$, $\dot{x}_c$, $y_c$, $\dot{y}_c$, $\beta$, $\dot{\beta}$, $\theta_L$, $\dot{\theta}_L$,$\theta_R$, $\dot{\theta}_R$, $N_L$, and $N_R$. Equations 15, 16, 34, 47, and 48 represent five second order different equations that can be used to solve for the first ten variables ($x_c$, $\dot{x}_c$, $y_c$, $\dot{y}_c$, $\beta$, $\dot{\beta}$, $\theta_L$, $\dot{\theta}_L$,$\theta_R$, $\dot{\theta}_R$), while Equations 32 and 33 can be used to solve for $N_L$, and $N_R$.

### 2.6 Steady State Motion along a Straight Line

In this paper, we focus on a special case of planar motion, i.e., *steady state motion along a straight line*, and the conditions necessary for the application of the holonomic constraint relating the linear and angular displacements ($x$ and $\theta$, respectively) of the helical drives.

While moving along a straight line with no failure of substrate, the degree of freedom of the system is reduced from three ($x_c$, $y_c$, and $\beta$) to one ($x_c$). The rover is assumed to be moving along the x-axis and therefore $y_c = 0, \dot{y}_c = 0$, $\ddot{y}_c = 0$, $\beta = 0$, $\dot{\beta} = 0$, and $\ddot{\beta} = 0$. Since the rover uses a differential

steering system, the angular displacements, velocities, and accelerations of the left and right helical drives have to be equal in magnitude while moving in a straight line, i.e., $\theta_L = \theta_R = \theta$, $\dot{\theta}_L = \dot{\theta}_R = \dot{\theta}$, and $\ddot{\theta}_L = \ddot{\theta}_R = \ddot{\theta}$. This is possible only if the external torques (applied by the motors) and normal forces (exerted by the surrounding substrate) on the left and right helical drives are equal in magnitude, i.e., $\vec{\tau}_{motor,HL,x} = \vec{\tau}_{motor,HR,x} = \vec{\tau}_{motor,x}$ and $N_L = N_R = N$.

Following these simplifications, the number of dependent variables in the dynamic model is reduced from twelve ($x_c$, $\dot{x}_c$, $y_c$, $\dot{y}_c$, $\beta$, $\dot{\beta}$, $\theta_L$, $\dot{\theta}_L$,$\theta_R$, $\dot{\theta}_R$) to five ($x_c$, $\dot{x}_c$, $\theta, \dot{\theta}, N$). The two second order differential equations and one algebraic equation used to solve for the five dependent variables are:

$$2 * N cos\varphi - 2 * F_1 sin\phi - 2 * F_2 sin\varphi = (m_{cc} + 2 * m_{HD}) * \ddot{x}_c \quad (49)$$

$$r * (-N sin\varphi - F_1 cos\phi - F_2 cos\varphi) + \vec{\tau}_{motor,,x} = \tilde{I}_{HD,x} \cdot \ddot{\theta} \quad (50)$$

$$r[-2 * N \cos\varphi + 2 * F_1 sin\phi + 2 * F_2 sin\varphi] = 0 \quad (51)$$

Equations 49, 50, and 51 are derived using Equations 15, 47, and 33, respectively, using the following notations: $F_{L1} = F_{R1} = F_1$; $F_{L2} = F_{R2} = F_2$; and $\phi_L = \phi_R = \phi$ in addition to the simplifications listed previously.

For a system in steady state motion, the net force and net torque acting on the system are equal to zero. Consequently, if said system has constant mass (such as the MAARCO rover), the linear and angular accelerations are equal to zero. Thus, for the MAARCO rover moving in a straight line in steady state, $\ddot{x}_c = 0$ and $\ddot{\theta} = 0$. This means the linear velocity of the system $\dot{x}_c$ and the angular velocities of both helical drives $\dot{\theta}$ remain constant and $x_c$ and $\theta$ can be calculated by simply integrating $\dot{x}_c$ and $\dot{\theta}$, respectively, over time. After implementing $\ddot{x}_c = 0$ and $\ddot{\theta} = 0$, Equations 49 and 51 are now equivalent and Equations 49 and 50 are algebraic equations (instead of second order differential equations). The normal/propulsive exerted by the surrounding substrate on the helical drives ($N$) can be calculated using Equation 49 (or Equation 51). Similarly, the driving torque ($\vec{\tau}_{motor,,x}$) required to maintain steady state motion along a straight line can be calculated using Equation 50 and the value of $N$.

### 2.7 Holonomic Constraint

The motion of MAARCO, a helical drives-based rover, while moving in a straight line is constrained 'holonomically' if the surrounding substrate does not fail under the shear stresses exerted by the helical drives. The motion of each helical drive resembles that of a "bolt through a threaded hole". In such a scenario, the linear displacement of the center of mass of the rover, $x_c$, and the number of rotations of the helical drives, $n$, are related by the following expression:

$$x_c = P \cdot n \quad (52)$$

where, $P$ is the pitch of the helical drives. The holonomic constraint shown in Equation 52 is used to eliminate a degree of freedom – $x_c$, in the dynamic model and the system of equations derived previously (Equations 49, 50, 51) is used to solve for the other dependent variables – namely, $N$ and $\theta$. However, if the substate fails under the stresses exerted by the helical drive, then the above holonomic constraint does not apply, and the linear displacement of the rover is less than $P * n$. The analysis of the locomotion dynamics of MAARCO when the substrate fails is out of the scope of this paper. However, the holonomically constrained locomotion of the rover, i.e., when $x_c = P \cdot n$ is valid, represents the best-case scenario and hence the most optimal operating condition in that the rover achieves maximum linear displacement of distance ($P$) per rotation, and hence warrants a detailed study of the conditions enabling such motion.

Additionally, when the holonomic constraint is active, the expression for the angle $\phi$ simplifies to $\phi = \frac{P}{r} = \varphi$. This is because the linear velocity of the rover and thereby the helical drives can be derived using Equation 52 and is equal to $\|\vec{v}_{L\ or\ R}\| = P \cdot \omega$.

### 2.8 Substrate Failure Check

In this section, we present the analysis for checking if the substrate fails under stresses exerted by the helical drives on the surrounding substrate. The forces acting on the substrate element located between two helical drives include:

1. *Normal force due to rover weight* ($\vec{N}_g$) – exerted by ballast
2. *Normal/propulsive force that results in forward motion of rover* ($\vec{N}_L$, $\vec{N}_R$, or $\vec{N}$) – exerted by blades
3. *Normal force due to stationary substrate wall* ($\vec{N}_w$) – exerted by substrate wall
4. *Friction force due to rover weight* $\vec{N}_g$ ($\overrightarrow{F_{L1}}$ , $\overrightarrow{F_{R1}}$, or $\overrightarrow{F_1}$) – exerted by ballast
5. *Friction force due to* $\vec{N}$ ($\overrightarrow{F_{L2}}$ , $\overrightarrow{F_{R2}}$, or $\overrightarrow{F_2}$) – exerted by blades
6. *Friction force due to substrate wall* ($\vec{F}_w$) – exerted by substrate wall

The friction forces due to substrate wall are also assumed to be kinetic friction forces are of the form $\vec{F}_{friction} = \mu_k \cdot \vec{F}_{Normal}$, where $\vec{F}_{Normal}$ is a function of the normal force due to the stationary wall The normal force $\vec{N}_w$ depends on the weight of the rover and the weight of the soil element, and is derived using the expression:

$$\vec{N}_w = (0.5 * (m_{cc} + 2 * m_{HD}) + m_{sub}) g\, \vec{k}_{\bar{o}} \quad (53)$$

where, $m_{sub}$ is the mass of the substrate element. The normal and shear stresses exerted by the forces are calculated using $\sigma\ (or\ \tau) = \frac{F}{A}$, where $\sigma$ is the normal stress, $\tau$ is the shear stress, $F$ is the normal or friction force, and $A$ is the substrate element surface area that the stress is exerted upon. Fig. 6 shows a schematic of the stresses exerted by the right helical drive on the substrate element. The stresses are assumed to act on the centroid of their respective surfaces. The area of each face and the mass of substrate element depend on the sinkage of the helical drives. In this analysis, the helical drive sinkage is assumed to be

constant. The normal compressive stresses acting on the top and bottom faces are assumed to be the average of the normal stresses due to the normal forces $\vec{N}_g$ and $\vec{N}_w$. Because the substrate element is in equilibrium, the shear stress due to $F_1$ acting on the top face and the shear stress due to $F_w$ acting on the bottom of fac are assumed to be equal in magnitude and opposite in direction. Using the frame of reference shown in Fig. 6, the stress tensor for an infinitesimally small cube-shaped element located inside the annulus shaped substrate element can be populated using the following expressions:

$$\sigma_x = -\sigma_R \tag{54}$$

$$\sigma_y = 0 \tag{55}$$

$$\sigma_z = -\frac{\sigma_g + \sigma_w}{2} = -\sigma_{g+w} \tag{56}$$

$$\tau_{xy} = 0 \tag{57}$$

$$\tau_{yz} = \tau_{R2} \tag{58}$$

$$\tau_{zx} = \frac{\tau_{R1} + \tau_w}{2} = \tau_{R1+w} \tag{59}$$

Populating the stress tensor using the above expressions gives us $S_{ij}$ a symmetric matrix:

$$S_{ij} = \begin{bmatrix} \sigma_x & \tau_{xy} & \tau_{zx} \\ \tau_{xy} & \sigma_y & \tau_{yz} \\ \tau_{zx} & \tau_{yz} & \sigma_z \end{bmatrix} = \begin{bmatrix} -\sigma_R & 0 & \tau_{R1+w} \\ 0 & 0 & \tau_{R2} \\ \tau_{R1+w} & \tau_{R2} & -\sigma_{g+w} \end{bmatrix} \tag{60}$$

The eigen values of $S_{ij}$ represent the principal stresses $(\sigma_1, \sigma_2, \sigma_3)$ acting on the substrate element. Because $S_{ij}$ is a real symmetric matrix, its eigen values will be real numbers [11]. The maximum shear and normal stresses acting on the substrate element are calculated using the principal stresses as follows:

$$\sigma_1, \sigma_2, \sigma_3 = eigen(S_{ij}) \tag{61}$$

$$Maximum\ Normal\ Stress = \sigma_{max} = \max(\sigma_1, \sigma_2, \sigma_3) \tag{62}$$

$$Minimum\ Normal\ Stress = \sigma_{min} = \min(\sigma_1, \sigma_2, \sigma_3) \tag{63}$$

$$Maximum\ Shear\ Stress = \tau_{max} = \pm\frac{\sigma_{max} - \sigma_{min}}{2} \tag{64}$$

Here, if the maximum shear stress ($\tau_{max}$) acting on the substrate element is greater than or equal to the shear strength of the substrate material ($\tau_{sub}$), i.e., $\tau_{max} \geq \tau_{sub}$, then the substrate element fails and the holonomic constraint in Equation 38 is invalid. However, if the $\tau_{max} < \tau_{sub}$, then the material does not fail, and the constraint is valid. The shear strength of the substrate is calculated using the Mohr-Coulomb criterion:

$$\tau_{sub} = c + \sigma_{max,shear} * \tan\phi_F \tag{65}$$

where, $c$ and $\phi_F$ are the apparent cohesion and internal shearing resistance of the substrate. These are substrate properties that are determined experimentally. $\sigma_{max,shear}$ is the normal stress acting on the surface of maximum shear stress, and is calculated using the principal stresses as follows:

$$Normal\ Stress\ at\ Max\ Shear = \sigma_{max,shear} = \frac{\sigma_{max} + \sigma_{min}}{2} \tag{66}$$

## 3. RESULTS AND DISCUSSION

The dynamic model and substrate failure analysis performed in the previous sections can be used to derive a design of the MAARCO that results in $x = P \cdot n$ motion while moving in a straight line in different types of substrates. The conditions for substrate failure depend only on the bulk properties of the substrate and dimensions and weight of the rover, while moving in a straight line in steady state.

As shown in Section 2.8, the conditions for substrate failure depend on the normal and shear stresses exerted by the rover, which in turn depend on the design of the helical drives, the weight of the rover, and the substrate density. The ballast diameter and blade height of the helical drives determine the surface area on which the various forces act as well as the amount of substrate present between two blades. Similarly, the overall weight of the rover, which consists of the central console representing the payload and the pair of helical drives, affects the normal and friction forces acting on the substrate. Hence, in this study, we determine the maximum possible payload ($m_{cc,max}$) that the rover can carry without failing the surrounding substrate as a function of the ballast diameter and blade height of the helical drives. This analysis is performed on four different substrates – dry sand, sandy loam, clayey soil, and snow, and the results are shown in Fig. 7-10, respectively. The data points shown in the four plots represent the maximum ~~payload~~ total masses for a set of ballast diameter, blade height, and substrate beyond which the substrate will fail under the loads exerted by the rover. The bulk properties of these substrates are shown in Table 1, while the rover properties that are kept constant throughout the analysis are shown in Table 2. The ballast diameter and blade height values used in this analysis were multiples of ballast diameter and blade height of helical drives used in a prototype designed and tested by the authors. The values of the baseline ballast diameter and blade height are 0.048 m and 0.009 m respectively. The mass of helical drives is assumed to be constant across the range of ballast diameters and blade heights. Additionally, the friction coefficients between the helical drives and all four substrates are assumed to be the same (as experiment and measurement of friction coefficients for all substrate is beyond the scope of this paper).

### 3.1 Effect of Ballast Diameter

The maximum payload increases with an increase in ballast diameter. This trend remains consistent throughout the four substrates under consideration. For a fixed sinkage, as the ballast diameter increases, the area of the ballast in contact with the substrate increases and therefore the normal and shear stresses exerted by the central cylinder (ballast) decrease. However, the reduction in stresses is not significant as the maximum payload that the substrate can withstand without failing only increases marginally. For example, in the case of dry sand, for a six-fold increase in ballast diameter, the maximum payload increases by only 3.9 kg for a fixed blade height of 0.5 times the baseline blade height.

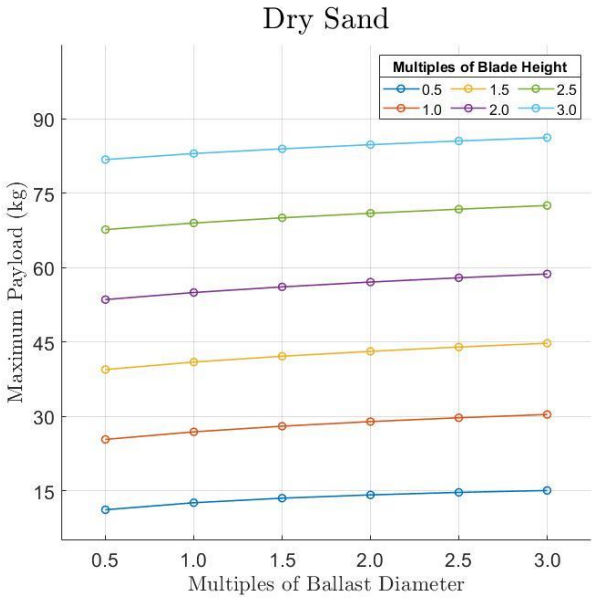


**FIGURE 7:** DISTRIBUTION OF MAXIMUM ROVER PAYLOAD AS A FUNCTION OF BALLAST DIAMETER AND BLADE HEIGHT WHILE MOVING ON DRY SAND

### 3.2 Effect of Blade Height

The maximum payload increases with an increase in blade height for all four substrates. However, compared to the ballast diameter, the increase is significantly higher. For example, in the case of dry sand, a six-fold increase in blade height results in an increase of 70.64 kg for a fixed ballast diameter corresponding to the 0.5 multiple case (brief explanation of how plots suggest so). This phenomenon can be explained as follows: a heavier payload results in a heavier rover which requires a greater amount of propulsive ($N$) to achieve and maintain $x = P \cdot n$ motion. A higher blade height results in a higher blade surface area for the $N$ and the friction force due to N, thereby resulting in lower normal and shear stresses exerted by the blades on the substrate element. Because the blade height directly affects the stresses resulting from $N$, it has a more prominent impact on the maximum payload.

### 3.3 Effect of $c$ and $\phi$

The apparent cohesion ($c$) and angle of internal shearing resistance ($\phi$) have a significant effect on the maximum payload. Substrates with a higher value of $c$ and/or $\phi$ result in a higher maximum payload. For example, sandy loam has a higher apparent cohesion (more than twice) compared to clayey soil, and therefore can sustain significantly higher maximum payloads without failure. Similarly, dry sand has a higher angle of internal shearing resistance than snow resulting in higher maximum payloads.

**Table 1.** Substrate Properties

| | $c$ (kPa) | $\phi$ (deg) | $\rho$ (kg/m3) |
|---|---|---|---|
| **Dry Sand** | 1.04 | 28 | 1638.3 |
| **Sandy Loam** | 5.17 | 11 | 1550 |
| **Clayey Sand** | 2.07 | 10 | 1400 |
| **Snow** | 1.03 | 19.7 | 125 |

### 3.4 Effect of $\rho$

The density ($\rho$) of the substrate affects the mass of the substrate element between two blades, which in turn affects the normal (or compressive) stress exerted by the stationary substrate wall on the element. A comparison of the plots of dry sand and snow shows that the density of substrate has an insignificant effect on the maximum payload. The density of dry sand is about 13 times that of snow, however, the maximum payload values across the range of ballast diameters and blade height differ only marginally.

**Table 2.** Rover and Substrate Parameters

| Property | Description | Value | Unit |
|---|---|---|---|
| $m_{HD}$ | Mass of HD | 2.25 | kg |
| $l_{HD}$ | Length of HD | 0.319 | m |
| $P$ | Pitch Length of HD | 0.0366 | m |
| $\varphi$ | Pitch Angle of HD | 10 | deg |
| $I_{HD}$ | Moment of Inertia of HD | 0.0012 | kg.m2 |
| $s$ | Sinkage | 0.0165 | m |
| $\mu_{k1}$ | Kinetic Friction Coefficient between HD and Substrate | 0.35 | - |
| $\mu_{k2}$ | Kinetic Friction Coefficient between Stationary and Moving Substrate | 0.2 | - |

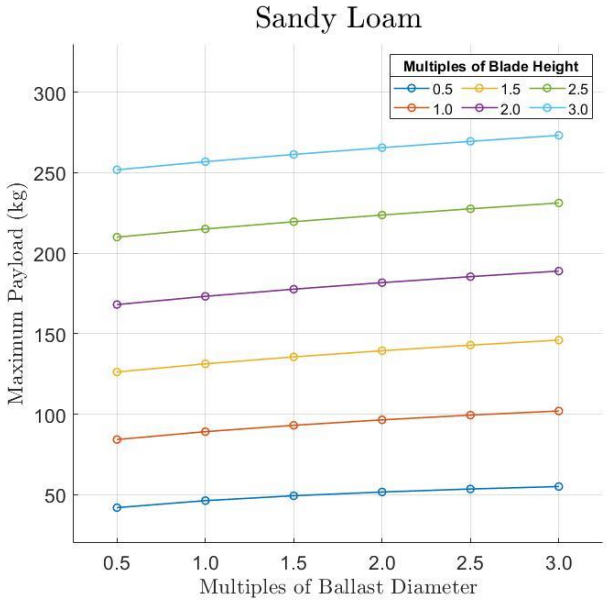


**FIGURE 8:** DISTRIBUTION OF MAXIMUM ROVER PAYLOAD AS A FUNCTION OF BALLAST DIAMETER AND BLADE HEIGHT WHILE MOVING ON SANDY LOAM

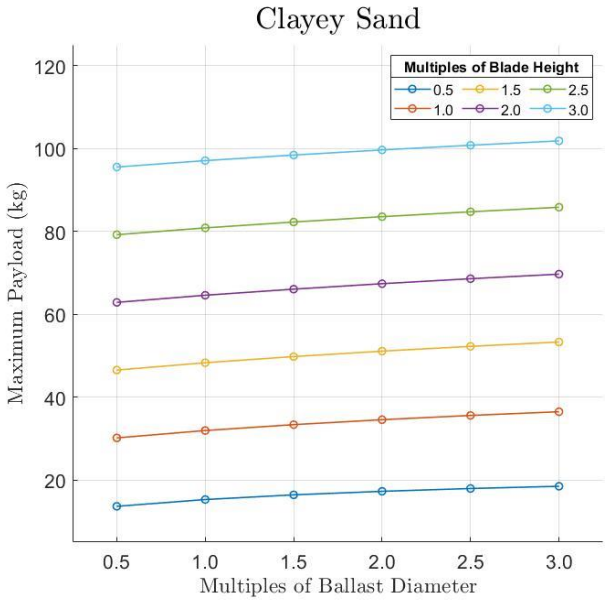


**FIGURE 9:** DISTRIBUTION OF MAXIMUM ROVER PAYLOAD AS A FUNCTION OF BALLAST DIAMETER AND BLADE HEIGHT WHILE MOVING ON CLAYEY SOIL

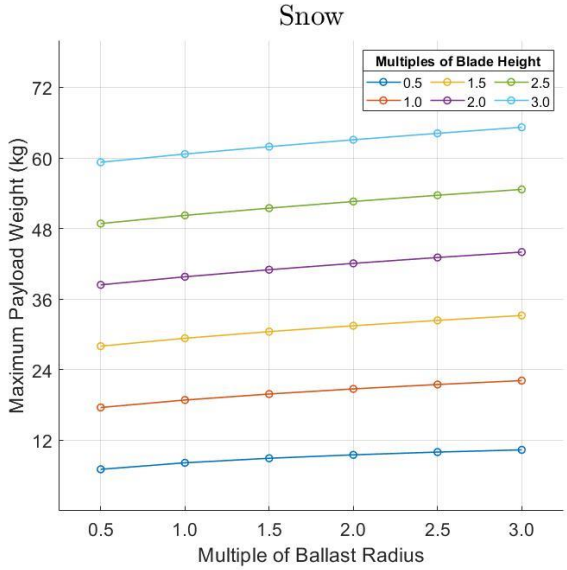


**FIGURE 10:** DISTRIBUTION OF MAXIMUM ROVER PAYLOAD AS A FUNCTION OF BALLAST DIAMETER AND BLADE HEIGHT WHILE MOVING ON SNOW

## 4. CONCLUSION

A planar locomotion dynamics model of a multi-terrain and amphibious robot designed for exploring the heterogeneous landscape of the Arctic has been derived. Additionally, the conditions necessary to achieve optimal locomotion performance, i.e., $x_c = P \cdot n$, while moving in a straight line have been derived. The dynamic model and substrate failure analysis have been used in unison to derive rover dimensions and weight resulting in $x_c = P \cdot n$ on different substrates.


## ACKNOWLEDGEMENTS

The authors gratefully acknowledge funding for this research provided by the National Science Foundation under award "MAARCO – Multi-terrain Amphibious ARCtic ExplOrer", award no. CMMI-2116216, which is managed by Dr. Alex Leonessa


## REFERENCES


[1] Pedersen, Liam, Michael Wagner, Dimitrios Apostolopoulos, and W. R. Whittaker. "Autonomous robotic meteorite identification in Antarctica." In *Proceedings 2001 ICRA. IEEE International Conference on Robotics and Automation (Cat. No. 01CH37164)*, vol. 4, pp. 4158-4165. IEEE, 2001.

[2] Akers, Eric L., Richard S. Stansbury, Torry L. Akins, and Arvin Agah. "Mobile robots for harsh environments: Lessons learned from field experiments." In *2006 World Automation Congress*, pp. 1-6. IEEE, 2006.

[3] Ray, Laura, Alexander Price, Alexander Streeter, Daniel Denton, and James H. Lever. "The design of a mobile robot for instrument network deployment in antarctica." In *Proceedings of the 2005 IEEE International Conference on Robotics and Automation*, pp. 2111-2116. IEEE, 2005.

[4] Nagaoka, Kenji, Masatsugu Otsuki, Takashi Kubota, and Satoshi Tanaka. "Terramechanics-based propulsive characteristics of mobile robot driven by Archimedean screw mechanism on soft soil." In *2010 IEEE/RSJ International Conference on Intelligent Robots and Systems*, pp. 4946-4951. IEEE, 2010.

[5] Thoesen, Andrew, Teresa McBryan, and Hamidreza Marvi. "Helically-driven granular mobility and gravity-variant scaling relations." *RSC advances* 9, no. 22 (2019): 12572-12579.

[6] He, Ding, and Li Long. "Design and analysis of a novel multifunctional screw-propelled vehicle." In *2017 IEEE International Conference on Unmanned Systems (ICUS)*, pp. 324-330. IEEE, 2017.

[7] Donohue, Brigid, Sumedh Beknalkar, Matthew Bryant, Andre Mazzoleni. "A Dynamic Model for Underwater Propulsion of an Amphibious Rover Developed From Kane's Method" In Press.

[8] Donohue, Brigid, Sumedh Beknalkar, Maria Aleman, Matthew Bryant, Andre Mazzoleni. "Modeling Underwater Propulsion of a Helical Drive Using Computational Fluid Dynamics for an Amphibious Rover" In Press.

[9] Vadlamannati, Ashwin, Sumedh Beknalkar, Dustin Best, Matthew Bryant, Andre Mazzoleni. "Design, Prototyping and Experiments Using Small-Scale Helical Drive Rover for Multi-Terrain Exploration" In Press.

[10] Lynch, Ryan, Sumedh Beknalkar, Riley Bishop, Arin Crow, Brigid Donohue, Cristian Pacheco-Cay, Alaina Smith, Andre Mazzoleni, Matthew Bryant. "Design and Construction of a Terrestrial Testing Rig for Experimentation and Analysis of Multi-Terrain Screw-Propelled Vehicle Dynamics and Performance" In Press.

[11] Clint, Maurice, and A. Jenning. "The evaluation of eigenvalues and eigenvectors of real symmetric matrices by simultaneous iteration." *The Computer Journal* 13, no. 1 (1970): 76-80.